Proceedings of the 11th Brazilian Congress of Thermal Sciences and Engineering -- ENCIT 2006
Braz. Soc. of Mechanical Sciences and Engineering -- ABCM, Curitiba, Brazil,- Dec. 5-8, 2006

Paper CIT06-0594

NUMERICAL SIMULATION OF THE TRANSONIC LAMINAR FLOW IN AIRFOILS WITH HIGH AMPLITUDE PLUNGING MOTIONS

Rúdner Lauterjung Queiroz
Universidade de Brasília, ENM – FT – UnB, Campus Universitário Darcy Ribeiro, Asa Norte, 70910-900, Brasília, DF, Brasil
rudner@gmail.com

Roberto Francisco Bobenrieth Miserda
Universidade de Brasília, ENM – FT – UnB, Campus Universitário Darcy Ribeiro, Asa Norte, 70910-900, Brasília, DF, Brasil
rfbm@unb.br

Abstract. *This work is a direct numerical simulation of the transonic laminar flow in airfoils with high amplitude plunging motions. The problem is solved for a non-inertial system of reference which is moving with the airfoil, and for this reason, the associated pseudo-force is included as a source in the momentum equation and the work done is also included as a source in the energy equation. This methodology allows the solution of high amplitude plunging motions, since the problem is solved from a non-inertial frame of reference which is moving with the airfoil and, for this reason, no grid deformation is needed to account for the motion. The compressible Navier-Stokes equations are solved using the skew-symmetric form of Ducros' shock-capturing algorithm, with fourth-order accuracy in space and third-order accuracy in time. Five cases are studied: the static airfoil and the plunging motions with amplitudes of 2.5%, 13%, 22% of the airfoil chord. For all the cases, the Reynolds number is 10,000, the Mach number of the free flow is 0.8 and the plunging frequency has same value of the vortex emission frequency of the static case. The numerical results show a very complex and unsteady interaction between the boundary layer, the detached vortex wake and the transonic shock-wave system for the four cases studied. There are also some characteristic shock phenomena at the last two cases.*

Keywords. *Transonic, Laminar Flow, Plunging Motion, High Amplitude*

1. Introduction

This work is aimed at the numerical simulation of the strong vortex-shock interaction that arises in the transonic flow over BGK-1 supercritical airfoil in laminar regime, submitted to plunging motion. This kind of interaction is typical of the unsteady aerodynamics of bodies in transonic flows, directly connected to limit cycle oscillations in transonic flows and flutter phenomena. Such phenomena are of high interest in the aerospace sciences.

The complex nature of these interactions demands numerical methods with shock-capturing schemes to obtain accurate results. In the case of plunging motions, a modified set of governing equations in order to simulate the oscillations of the body is also necessary.

Using this methodology, the study of transonic flows started with the investigation of Transonic Buffet in airfoils (Bobenrieth Miserda *et al*., 2004) and the investigation of transonic flows in a near-base (Bobenrieth Miserda and Mendonça, 2005). After that, the investigation of the transonic flow with plunging and pitching motions (Lauterjung *et al*., 2005 and Bobenrieth Miserda *et al*., 2006) has begun. Meanwhile, the subsonic flow with plunging motion (Bobenrieth Miserda and Carvalho, 2006) and with pitching motion (Guimarães and Silva, 2005) were also being studied. In order to start exploring turbulent flows, the transonic cylinder (Bobenrieth Miserda and Leal, 2006) was also investigated.

2. Mathematical Model

In this work, the system of equations is written using a non-inertial frame of reference which is fixed to the plunging airfoil. The effect of this motion is accounted by a pseudo-force term in the right-hand side of the momentum equation which acts as a body force (Batchelor, 1983). In similar manner, the work done by this pseudo-force is accounted by a pseudo-work term in the right-hand side of the energy equation. With these considerations, the nondimensional form of the Navier-Stokes equations can be written as:

$$\frac{\partial \rho}{\partial t} + \frac{\partial}{\partial x_i}(\rho u_i) = 0 \tag{1}$$

$$\frac{\partial}{\partial t}(\rho u_i) + \frac{\partial}{\partial x_j}(\rho u_i u_j) = -\frac{\partial p}{\partial x_i} + \frac{\partial \tau_{ij}}{\partial x_j} + f_i \tag{2}$$

$$\frac{\partial}{\partial t}(\rho e_T)+\frac{\partial}{\partial x_i}(\rho e_T u_i)=-\frac{\partial}{\partial x_i}(p u_i)+\frac{\partial}{\partial x_i}(t_{ij}u_j)-\frac{\partial q_{x_i}}{\partial x_i}+f_i u_i \tag{3}$$

All variables are in nondimensional form and have their usual meaning, i.e., ρ is the density, t is the nondimensional time, x_i is the i-direction spatial coordinate, u_i is the i-direction component of the velocity vector, p is the pressure, t_{ij} denotes the viscous stress tensor, e_T is the total energy per unit of mass, q_{xi} is the heat-flow density in the i-direction and f_i is the pseudo-force due to the plunging motion.

The nondimensional form of the flow variables and properties are defined as

$$\begin{aligned} &x_i=\frac{x_i^*}{c^*},\quad u_i=\frac{u_i^*}{U_\infty^*},\quad t=\frac{t^*}{c^*/U_\infty^*},\quad p=\frac{p^*}{\rho_\infty^*\left(U_\infty^*\right)^2},\quad \rho=\frac{\rho^*}{\rho_\infty^*},\quad e_T=\frac{e_T^*}{\left(U_\infty^*\right)^2},\\ &m=\frac{m^*}{m_\infty^*},\quad e=\frac{e^*}{\left(U_\infty^*\right)^2},\quad e_k=\frac{e_k^*}{\left(U_\infty^*\right)^2},\quad c_v=\left[\frac{T_\infty^*}{\left(U_\infty^*\right)^2}\right]c_v^*,\quad T=\frac{T^*}{T_\infty^*}, \end{aligned} \tag{4}$$

where the asterisk denotes dimensional quantities, c^* is the chord of the airfoil, μ^* is the dynamic viscosity, T^* is the temperature. U_∞^*, T_∞^*, ρ_∞^* and μ_∞^* are, respectively, the velocity, temperature, density and dynamic viscosity of the undisturbed flow. The nondimensional viscous stress tensor is given by

$$t_{ij}=\frac{1}{\mathrm{Re}}\left(\mu S_{ij}\right)=\frac{1}{\mathrm{Re}}\left\{\mu\left[\left(\frac{\partial u_i}{\partial x_j}+\frac{\partial u_j}{\partial x_i}\right)-\frac{2}{3}\delta_{ij}\frac{\partial u_k}{\partial x_k}\right]\right\} \tag{5}$$

where δ_{ij} is the Kronecker delta. The Reynolds number is defined as

$$\mathrm{Re}=\frac{\rho_\infty^* U_\infty^* c^*}{\mu_\infty^*}. \tag{6}$$

Defining e as the nondimensional internal energy per unit of mass, e_k as the nondimensional kinetic energy per unit of mass and c_v as the nondimensional specific heat at constant volume, the total energy is given by the sum of the internal and kinetic specific energy as

$$e_T=e+e_k=c_v T+\frac{u_i u_i}{2} \tag{7}$$

and the nondimensional heat-flux density is

$$q_{x_i}=-\frac{\mu}{(\gamma-1)M^2\,\mathrm{Re}\,\mathrm{Pr}}\left(\frac{\partial T}{\partial x_i}\right) \tag{8}$$

where the M and Pr are the Mach and the Prandtl numbers, respectively, and are defined as

$$M=\frac{U_\infty^*}{\sqrt{\gamma R^* T_\infty^*}},\qquad \mathrm{Pr}=\frac{c_p^*}{k_\infty^*}\mu_\infty^* \tag{9}$$

where γ is the specific heat ratio, R^* is the specific gas constant, c_p^* is the specific heat at constant pressure and k_∞^* is thermal conductivity of the undisturbed flow.

In this work, the Prandtl number is considered a constant with the value $\mathrm{Pr}=0.72$. For a thermally and calorically perfect gas, the nondimensional equation of state can be written as

$$p=(\gamma-1)\rho\, e \tag{10}$$

and

$$T = \frac{g\ M^2 p}{r} \tag{11}$$

The nondimensional molecular viscosity is obtained using Sutherland's formula, where C_1 and C_2 are the nondimensional first and second gas constants,

$$m = C_1 \frac{T^{3/2}}{T + C_2}, \qquad C_1 = \left[\frac{\left(T_\infty^*\right)^{1/2}}{m_\infty^*}\right] C_1^*, \qquad C_2 = \frac{C_2^*}{T_\infty^*}. \tag{12}$$

The pseudo-force f_i, which appears in Eqs. (2) and (3), accounts for the two types of motion when the Navier-Stokes equations are written for a non-inertial frame or reference. When the plunging motion is imposed, and its linear amplitude is sinusoidal in time, the components of the pseudo-force, f_i, are given by

$$f_i = \frac{1}{2} r A_i w_i^2 \sin\left(w_i t\right) \tag{13}$$

The nondimensional maximum amplitude, A_i, and angular frequency, w_i, of the plunging motion are defined as

$$A_i = \frac{A_i^*}{c^*}, \qquad w_i = \frac{w_i^*}{U_\infty^* / c^*}. \tag{14}$$

The boundary conditions at the wall of the two-dimensional airfoil are a no-slip condition for the velocity field, an adiabatic wall for the temperature field and a null gradient in the normal direction at the wall for the pressure field.

3. Numerical Method

Since the geometry of interest is a two-dimensional airfoil and the flow around it is laminar, the two-dimensional form of the Navier-Stokes equations is used. In order to numerically solve these equations using a finite volume approach associated with a fixed grid, Eqs. (1), (2) and (3) are written in the following vector form (Anderson, 1983):

$$\frac{\partial \mathbf{U}}{\partial t} + \frac{\partial \mathbf{E}}{\partial x} + \frac{\partial \mathbf{F}}{\partial y} = \mathbf{R} \tag{15}$$

where **U** is the nondimensional conservative-variables vector, **E** and **F** are the nondimensional flux vectors. These vectors are given by

$$\mathbf{U} = \begin{bmatrix} r \\ ru \\ rv \\ re_T \end{bmatrix}, \quad \mathbf{E} = \begin{bmatrix} ru \\ ru^2 + p - t_{xx} \\ ruv - t_{xy} \\ (re_T + p)u - ut_{xx} - vt_{xy} + q_x \end{bmatrix}, \quad \mathbf{F} = \begin{bmatrix} rv \\ rvu - t_{xy} \\ rv^2 + p - t_{yy} \\ (re_T + p)v - ut_{xy} - vt_{yy} + q_y \end{bmatrix}, \tag{16}$$

where *u* and *v* are, respectively, the nondimensional component of the velocity vector in the *x*-direction and *y*-direction.

In this work, the plunging motion of the airfoil is imposed in the *y*-direction, and consequently, for this case the nondimensional **R** vector, which is associated with the plunging motion, is

$$\mathbf{R} = \begin{bmatrix} 0 \\ 0 \\ \frac{1}{2} r A_y w^2 \sin\left(w_y t\right) \\ \frac{1}{2} r A_y w^2 \sin\left(w_y t\right) v \end{bmatrix}. \tag{17}$$

Defining the flux tensor Π as

$$\Pi = \mathbf{E} \otimes \mathbf{i} + \mathbf{F} \otimes \mathbf{j} \tag{18}$$

where **i** and **j** are unit vectors in the *x*-direction and *y*-direction. Eq. (15) can be rewritten as

$$\frac{\partial \mathbf{U}}{\partial t} + \nabla \cdot \Pi = \mathbf{R} \tag{19}$$

Integrating the above equation over the control volume *V*, and applying the divergence theorem to the first term of right-hand side results

$$\frac{\partial}{\partial t}\int_V \mathbf{U}\, dV = -\int_V (\nabla \cdot \Pi)\, dV + \int_V \mathbf{R}\, dV = -\int_S (\Pi \cdot \mathbf{n})\, dS + \int_V \mathbf{R}\, dV \tag{20}$$

Defining the volumetric mean of vectors **U** and **R** in the control volume *V* as

$$\overline{\mathbf{U}} \equiv \frac{1}{V}\int_V \mathbf{U}\, dV, \qquad \overline{\mathbf{R}} \equiv \frac{1}{V}\int_V \mathbf{R}\, dV, \tag{21}$$

The upper bar means volumetric mean of the variable. Eq. (20) is written as

$$\frac{\partial \overline{\mathbf{U}}}{\partial t} = -\frac{1}{V}\int_S (\Pi \cdot \mathbf{n}) dS + \overline{\mathbf{R}} \tag{22}$$

For the volume (i, j), the first-order approximation of the temporal derivative is given by

$$\left(\frac{\partial \overline{\mathbf{U}}}{\partial t}\right)_{i,j} = \frac{\Delta \overline{\mathbf{U}}_{i,j}}{\Delta t} + O(\Delta t) \tag{23}$$

and the temporal approximation of Eq. (22) for a quadrilateral and two -dimensional control volume is

$$\Delta \overline{\mathbf{U}}_{i,j} = -\frac{\Delta t}{V_{i,j}}\left[\int_{S_{i+1/2}} (\Pi \cdot \mathbf{n})\, dS + \int_{S_{i-1/2}} (\Pi \cdot \mathbf{n}) dS + \int_{S_{j+1/2}} (\Pi \cdot \mathbf{n}) dS + \int_{S_{j-1/2}} (\Pi \cdot \mathbf{n}) dS\right] + \Delta t\, \overline{\mathbf{R}} \tag{24}$$

where $S_{i+1/2}$ is the common surface between volume (i, j) and volume $(i+1, j)$, **n** is the normal unit vector, *Dt* is the nondimensional time step. Defining

$$F\left(\overline{\mathbf{U}}\right)_{i,j} = (\Pi \cdot \mathbf{S})_{i+1/2} + (\Pi \cdot \mathbf{S})_{i-1/2} + (\Pi \cdot \mathbf{S})_{j+1/2} + (\Pi \cdot \mathbf{S})_{j-1/2} \tag{25}$$

the spatial approximation of Eq. (24) is

$$\Delta \overline{\mathbf{U}}_{i,j} = -\frac{\Delta t}{V_{i,j}}\left[F\left(\overline{\mathbf{U}}\right)_{i,j} - D\left(\overline{\mathbf{U}}\right)_{i,j}\right] + \Delta t\, \overline{\mathbf{R}} \tag{26}$$

where $D\left(\overline{\mathbf{U}}\right)_{i,j}$ is an artificial dissipation. It is important to note that Eq. (26) is a spatial approximation of Eq. (24) because tensor Π is considered constant over each of the four control surfaces that define the control volume. In order to calculate $F\left(\overline{\mathbf{U}}\right)_{i,j}$, the flux of tensor Π trough the control surfaces must be calculated. The explicit form of this calculation as well as the implementation of the artificial dissipation, $D\left(\overline{\mathbf{U}}\right)_{i,j}$, is given by Bobenrieth Miserda and Mendonça (2005).

In order to advance Eq. (26) in time, a third-order Runge-Kutta is used as proposed by Shu (Yee, 1997). This yield to

$$\overline{\mathbf{U}}^1 = \overline{\mathbf{U}}^n - \frac{\Delta t}{V_{i,j}}\left[F\left(\overline{\mathbf{U}}^n\right) - D\left(\overline{\mathbf{U}}^n\right)\right] + \Delta t\, \overline{\mathbf{R}}^n, \tag{27}$$

$$\overline{\mathbf{U}}^2 = \frac{3}{4}\overline{\mathbf{U}}^n + \frac{1}{4}\overline{\mathbf{U}}^1 - \frac{1}{4}\left\{\frac{\Delta t}{V_{i,j}}\left[F\left(\overline{\mathbf{U}}^1\right) - D\left(\overline{\mathbf{U}}^1\right)\right] + \Delta t\,\overline{\mathbf{R}}^1\right\}, \tag{28}$$

$$\overline{\mathbf{U}}^{n+1} = \frac{1}{3}\overline{\mathbf{U}}^n + \frac{2}{3}\overline{\mathbf{U}}^2 - \frac{2}{3}\left\{\frac{\Delta t}{V_{i,j}}\left[F\left(\overline{\mathbf{U}}^2\right) - D\left(\overline{\mathbf{U}}^2\right)\right] + \Delta t\,\overline{\mathbf{R}}^2\right\}. \tag{29}$$

As used in this work, the numerical method is fourth-order accurate in space and third-order accurate in time.

4. Results

For all cases studied in this work the Reynolds number is 10,000, and the characteristic length is the chord of the airfoil, c^*. The Mach number of the free flow is 0.80 and the angle of attack is 0 degrees. A c-grid is used, where 920 control volumes discretize the airfoil surface. The smallest grid size is $5.0\text{x}10^{-4}c^*$, and it is located at the leading-edge surface. The grid extends $10c^*$ in the upper and lower normal directions, and approximately $10c^*$ in the upstream and downstream directions. The total number of control volumes for this grid is 324,000, resulting in a problem with 1,296,000 degrees of freedom.

Four cases are studied. For the first case the airfoil is studied with no plunging motion. From the second to the fourth case, the reduced frequencies for the plunging motion, w_y, are the same and equal to 11.33. This value results in motions with a frequency equal to the vortex-emission frequency of the static case for this airfoil in 0° of angle of attack, obtained in the first case. The amplitudes used in the second, third and fourth cases are respectively 2.5%, 13.0% and 22% of the chord, which gives an maximum reference Mach number (resultant of the sum of the free flow velocity and the plunging velocity), M_{ref}, of 0.81, 1.0 and 1.3, respectively.

The visualizations presented on this work are the nondimensional magnitude of the density gradient, called *pseudo-Schlieren* in order to be compared with experimental gradient visualizations, called *Schlieren* visualizations. The density gradient was chosen in order to emphasize the high compressible nature of the cases. The pressure gradient and the temperature gradient are very similar, except by the intensity of some phenomena.

Figure 1 shows a region of the computational domain in conjunction with a magnified view showing the resolution of the computational grid at the trailing edge, which has the same order of resolution at the leading edge.

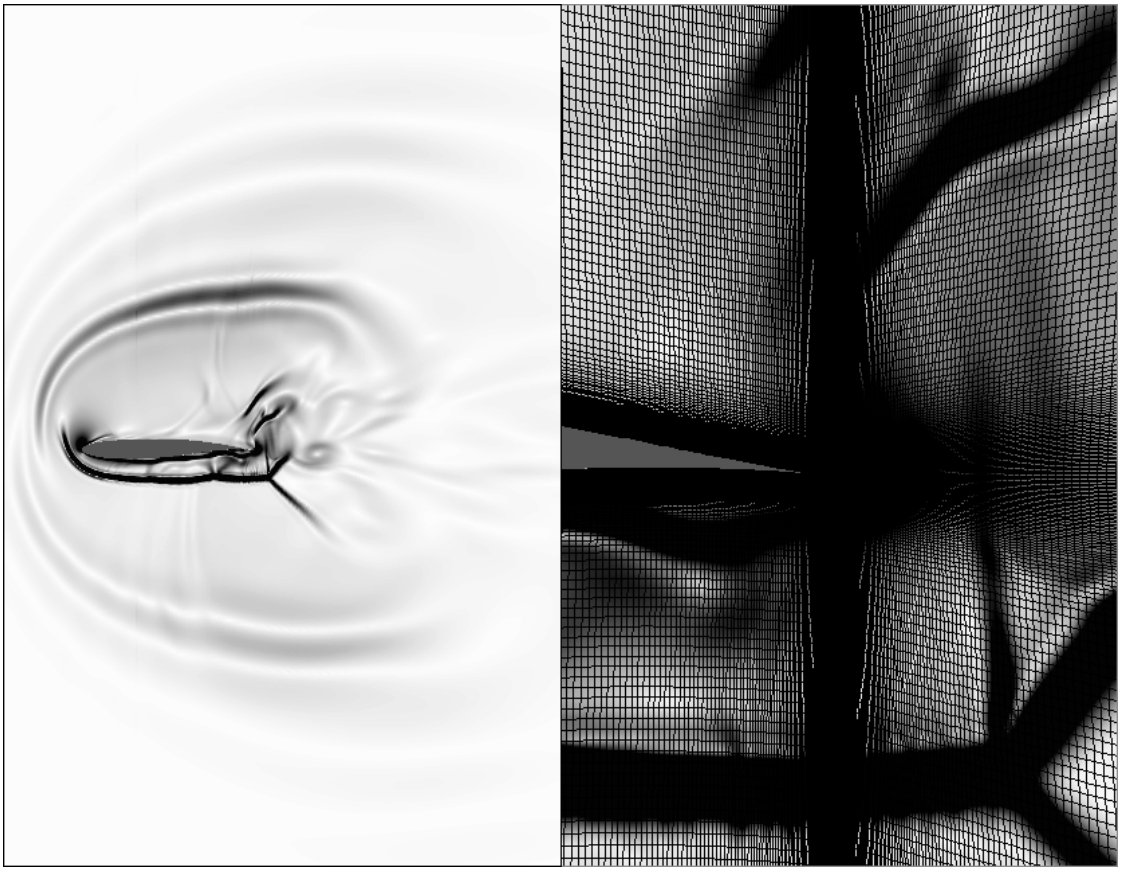

Figure 1. Flow visualization for $A_y = 0.22$. The variable plotted is the nondimensional magnitude of the density gradient. White corresponds to 0.0 and black to 10.0.

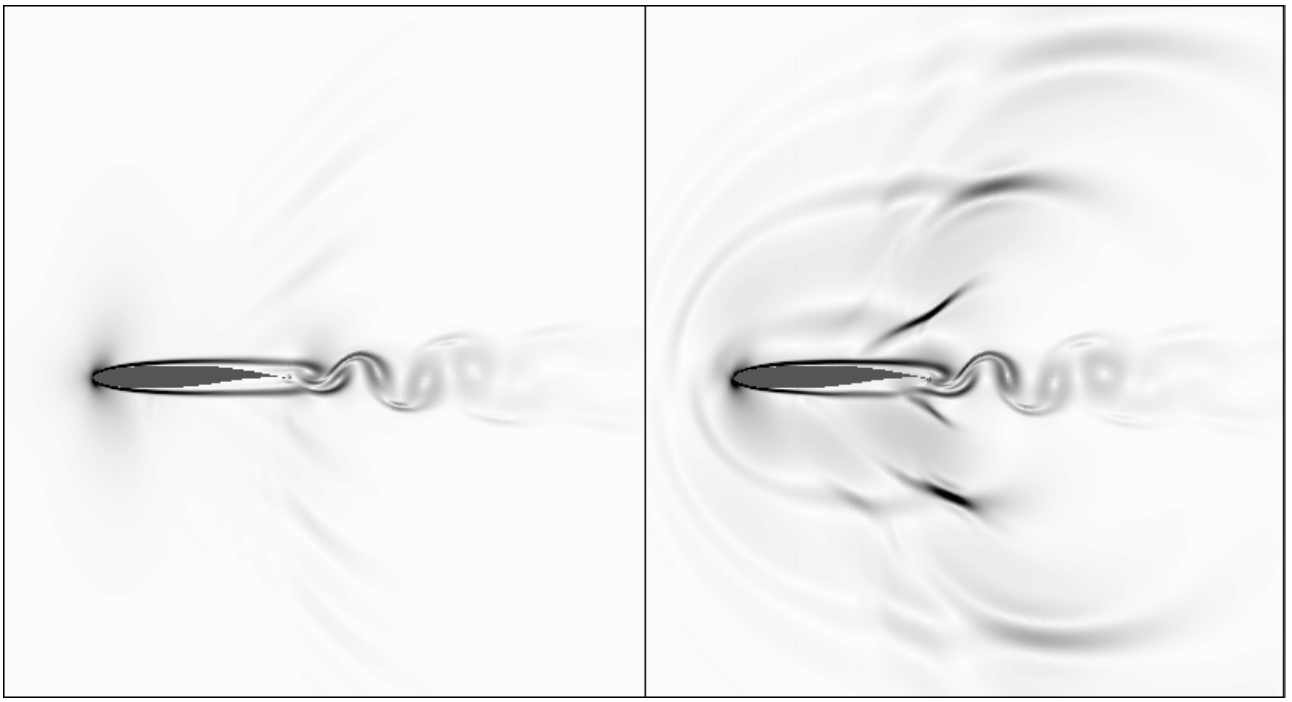

Figure 2. Flow visualization for $A_y = 0.0$ (left) and $A_y = 0.025$ (right). The variable plotted is the nondimensional magnitude of the density gradient. White corresponds to 0.0 and black to 6.0.

Figure 2 shows the visualization for an instant of the static and 2.5% plunging motion. In both cases, the visualization shows some aeroacoustic waves generated by the vortex emission at the trailing edge. In the plunging case (right), the visualization shows some acoustic waves due to the oscillation of the body and some lambda shock waves of short lifetime which appears near the trailing edge, that loose energy and becomes aeroacoustic waves propagating on the field with the plunging acoustic waves. In both cases, the skew-symmetric vortex street is very we ll defined.

Figure 3. Flow visualization for $A_y = 0.13$ (left) and $A_y = 0.22$ (right) for an instant of downward velocity. The variable plotted is the nondimensional magnitude of the density gradient. White corresponds to 0.0 and black to 10.0.

Figure 3 shows the visualization for an instant of downward velocity of the 13% and 22% plunging motions. In both cases, the visualization shows shock waves, emitted by the oscillation of the body, they loose energy and become acoustic waves propagating on the field, as well as some lambda shocks, near the trailing edge, and connecting shocks,

between the vortexes emitted at the downstream. Those very different characteristics of the flow cause some variation at the lift and drag coefficients as shown next.

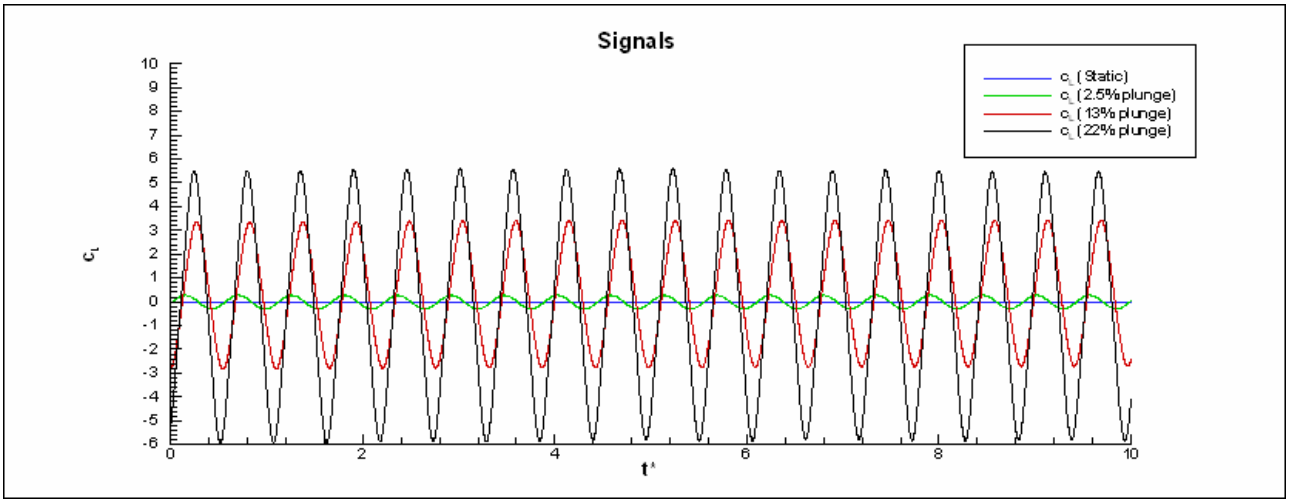

Figure 4. Unsteady lift coefficients as function of time. The blue, green, red and black colors correspond to the static, 2.5%, 13% and 22% of plunge cases, respectively.

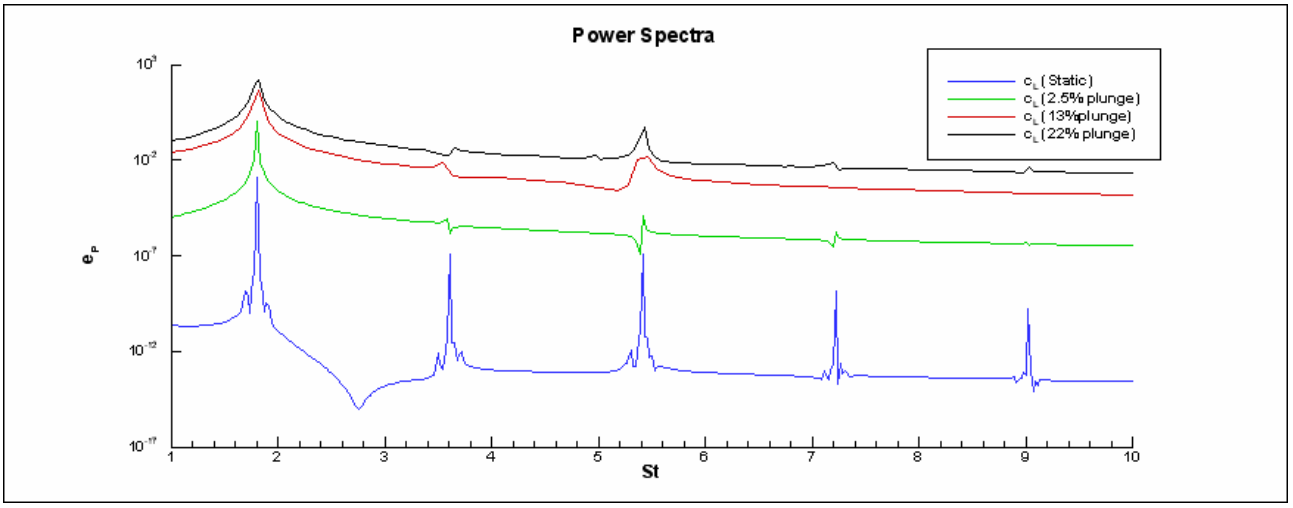

Figure 5. Power Spectra for the unsteady lift coefficients.

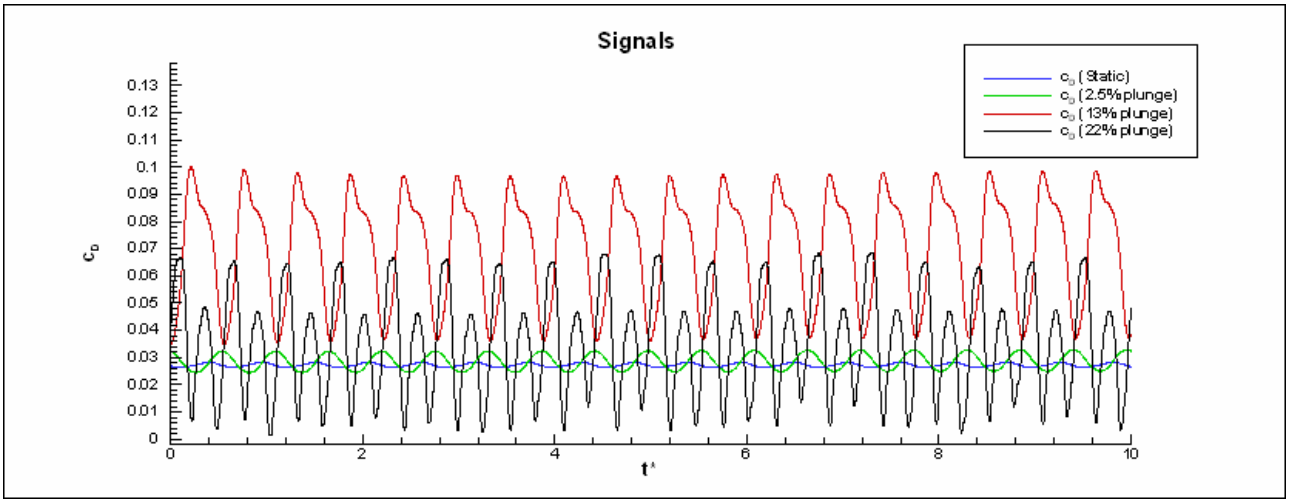

Figure 6. Unsteady drag coefficients as function of time. The blue, green, red and black colors correspond to the static, 2.5%, 13% and 22% of plunge cases, respectively.

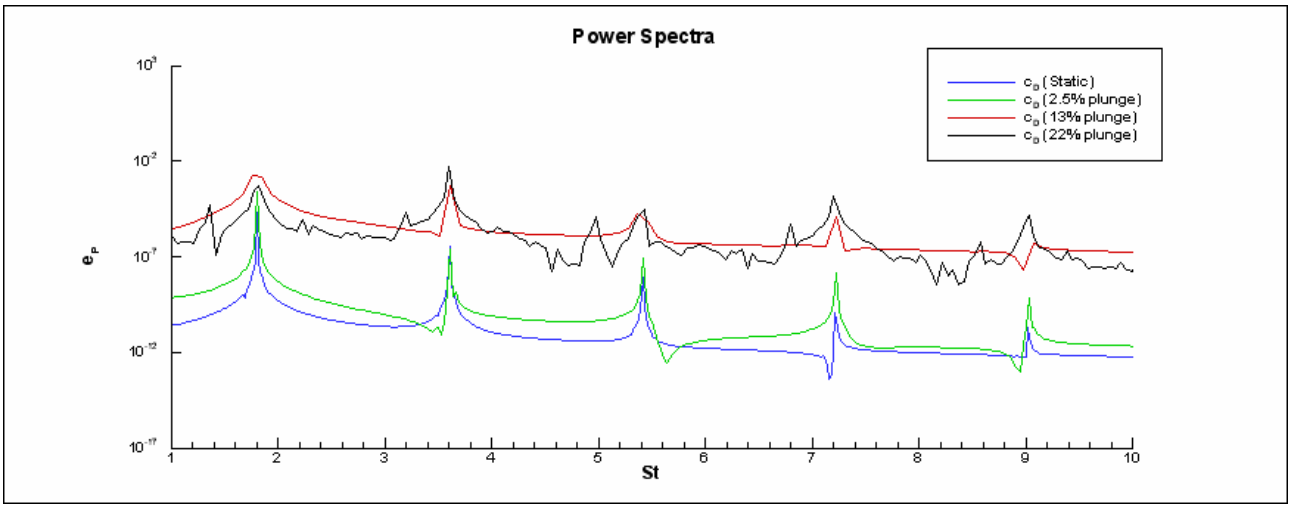

Figure 7. Power Spectra for the unsteady drag coefficients.

As the lift coefficient signals show, the variation of amplitude of the plunging motion seems to only change the amplitude of the lift coefficient fluctuation, keeping the mean value of the lift coefficient the same as its frequency of fluctuation. The power spectra show that there is one characteristic frequency and sub-harmonics of same values on the four cases studied. It shows also that all the cases are non-chaotic, in the lift coefficient point of view. But as the drag coefficient signals show, the behavior of the system changes drastically between the cases two and three.

In the first two cases, the mean value of the drag coefficient is the same, as well as the frequency of its fluctuation. The curves look like sinusoidal ones and are non-chaotic. There is one main value of frequency, with sub-harmonics, which are the same for both cases.

In the third case, the mean value of the drag coefficient rises considerably, as well as its fluctuation. There is still one main frequency, which is the same of the first two cases, and sub-harmonics. The curve is still non-chaotic, but it does not look like sinusoidal anymore.

In the fourth case, the mean value of the drag coefficient is reduced. There are two main frequencies, the power spectra show that the first one has the same value of the other cases and the second one is twice the value of the first one, but this frequency has more energy than the first one. There is also a broader distribution of the energy in the power spectrum, but with peaks on those two frequencies and their sub-harmonics, showing a pre-chaotic behavior.

5. Conclusions

A methodology is proposed in order to simulate the transonic laminar flow around the BGK-1 airfoil with imposed plunging motions, some with considerable amplitudes. It is based on the methodology proposed by Bobenrieth Miserda and Mendonça (2005), with the addition of pseudo-force and pseudo-work terms in the momentum and energy equations, respectively, in order to solve the system of governing equations from a non-inertial frame of reference which is moving with the airfoil, as proposed by Bobenrieth Miserda *et al.* (2006).

The dynamic response of the system is different when it is referenced to the lift coefficient to when it is referenced to the drag coefficient. When the lift coefficient is in sigh, there is no greater change when the amplitude is increased, causing just an increase on the fluctuation of the mean value, which was kept the same for all the cases studied. This simple change did not correspond to a very different nature of the flows, as seen on the visualizations, which gave the idea to investigate the signals of the drag coefficient.

When the drag coefficient is in sigh, the cases could be separated in two groups. In the first group of cases (the first and second cases), the increase of amplitude did only increase the fluctuation of the mean value of the drag coefficient, which was the same response seen at the lift coefficient study. But in the second group of cases (the third and fourth cases), the dynamic response became very different. In the third case, the mean value has increased and the curve was not sinusoidal anymore. In the fourth case, the mean value has decreased and other frequencies appeared in the response.

These differences may be related to the fact that in the third case, the reference Mach number is sonic, increasing the supersonic regions, as well as the number of shock waves, in many directions of the flow-field, such as connecting shocks, lambda shocks and other shock waves and phenomena. The appearance of those new shock waves in other directions and the level of energy associated to those flows may be also some reasons of these differences, which caused those differences on the drag coefficient dynamic response.

6. References

Anderson, D.A., Tannehill, J.C. and Pletcher, R.H., 1983, "Computational Fluid Mechanics and Heat Transfer", Hemisphe Publishing Corporation, New York.

Batchelor, C.K., 1983, "An introduction to Fluid Dynamics", University Press, Cambridge.

Bobenrieth Miserda, R.F., Jalowitzki, J.R., Lauterjung Q., R., and Mendonça, A.F. de, 2004, "Numerical Simulation of the Laminar Transonic Buffet in Airfoils", 10th Brazilian Congress of Thermal Sciences and Engineering – ENCIT 2004, CIT04-0609, Rio de Janeiro, Rio de Janeiro.

Bobenrieth Miserda, R.F., and Mendonça, A.F. de, 2005, "Numerical Simulation of the Vortex-Shock Interactions in a Near-Base Laminar Flow", AIAA 43rd Aerospace Sciences Meeting and Exhibit, AIAA 2005-0316, Reno, Nevada.

Bobenrieth Miserda, R.F., and Carvalho, A.R., 2006, "On the Effect of the Plunging Velocity over the Aerodynamic Forces for an Airfoil in Subsonic Laminar Flow", AIAA 44th Aerospace Sciences Meeting and Exhibit, AIAA 2006-0453, Reno, Nevada.

Bobenrieth Miserda, R.F., and Leal, R.G., 2006, "Numerical Simulation of the Unsteady Aerodynamic Forces over a Circular Cylinder in Transonic Flow", AIAA 44th Aerospace Sciences Meeting and Exhibit, AIAA 2006-1408, Reno, Nevada.

Bobenrieth Miserda, R.F., Lauterjung Q., R., and Jalowitzki, J.R., 2006, "On the Effect of the Plunging and Pitching Motions over the Dynamic Response of an Airfoil in Transonic Laminar Flow", AIAA 44th Aerospace Sciences Meeting and Exhibit, AIAA 2006-0452, Reno, Nevada.

Guimarães, R., and Silva, T., 2005, "Simulação Numérica do Escoamento Transônico Laminar em Aerofólios com Oscilação Angular", Relatório de Projeto de Graduação, Departamento de Engenharia Mecânica, Universidade de Brasília, Brasília, Distrito Federal.

Lauterjung Q., R., Jalowitzki, J.R., and Bobenrieth Miserda, R.F., 2005, "Numerical Simulation of the Transonic Laminar Flows in Airfoils with Pitching and Plunging Motion", 18th International Congress of Mechanical Engineering – COBEM 2005, COBEM2005-2431, Ouro Preto, Minas Gerais.

Yee, H.C., 1997, "Explicit and Implicit Multidimensional Compact High-Resolution Shock-Capturing Methods: Formulation", Journal of Computational Physics, Vol. 131, pp. 216-232.

7. Copyright Notice